Atomic data from the Iron Project

XXXVII. Electron impact excitation collision strengths and rate coefficients for Fe VI*

G.X. Chen and A.K. Pradhan

Department of Astronomy, The Ohio State University, Columbus, OH 43210, U.S.A.
Internet: chen@astronomy.ohio-state.edu

Abstract. Collision strengths and Maxwellian-averaged rate coefficients have been calculated for 3 160 non-vanishing transitions among 80 fine structure levels, dominated by configurations $3d^3$, $3d^24s$, and $3d^24p$ in Fe VI. Collision strengths are calculated using the R-matrix method with a 34-term close-coupling target expansion and for electron energies up to 10 Rydbergs. Detailed comparisons of rate coefficients are presented with the relativistic Breit-Pauli calculations using a 19-level expansion corresponding to the first 8 LS terms dominated by the ground configuration $3d^3$. For the low-lying transitions of practical interest there is excellent agreement, better than 10%, among three sets of rate coefficients calculated using the 34-term and 8-term non-relativistic calculations and the 19-level Breit-Pauli calculation, indicating that (i) the relativistic effects are not too significant, and (ii) the numerical uncertainties associated with the resolution of the extensive resonances in the collision strengths are small. Rate coefficients are tabulated in a range of temperatures, $10^4 - 10^6$ K, where Fe VI is normally abundant in radiatively photoionized or collisionally ionized plasmas sources. A brief discussion of the calculations and sample results are given. The present rates for Fe VI are expected to find applications in UV spectral diagnostics of hot stellar sources and planetary nebulae.

Key words: atomic data — white dwarfs — planetary nebulae

1. Introduction

Previous calculations on the low-ionization stages of iron have been carried out by the group at Ohio State for Fe II (Zhang & Pradhan 1995b), Fe III (Zhang 1996), and Fe IV (Zhang & Pradhan 1997). Whereas these ionization states of iron are the dominant species in gaseous nebulae and photoionized H II regions in general, Fe VI emission lines could also form in somewhat hotter sources such as from hot white dwarfs (Jordan et al. 1995). The [Fe VI] lines are observed in the optical spectra of relatively hot H II regions, such as the high-excitation planetary nebula NGC 6741 studied by Hyung & Aller (1997). Numerical simulation of spectral emission from such complex atomic species requires non-local thermodynamic equilibrium (NLTE) calculations involving many atomic levels (Koester 1995).

With the exception of two calculations two decades ago, there are no other calculations of electron impact excitation of Fe VI in literature (see the review by Pradhan 1994). It is difficult to calculate the relativistic effects together with the electron correlation effects in this complex atomic system and coupled channel calculations necessary for such studies are very computer intensive. The two previous sources for the excitation rates of Fe VI are the close coupling (CC) calculations by Garstang et al. (1978) and the distorted-wave (DW) calculations by Nussbaumer & Storey (1978). Although the Garstang et al. (1978) calculations were in the CC approximation, they used a very small basis set and did not obtain the resonance structures; their results are given only for the averaged values. The Nussbaumer & Storey (1978) calculations were in the DW approximations that does not enable a treatment of resonances. Therefore neither set of calculations included resonances or the coupling effects due to higher configurations. Owing primarily to these factors we find that the earlier data are in lower by several factors (discussed later) when compared to the new Fe VI rates presented herein.

The earlier studies on Fe III (Zhang & Pradhan 1995a) and Fe IV (Zhang & Pradhan 1997) using the nonrelativistic (NR) and Breit-Pauli R-matrix (BPRM) methods show that the relativistic effects are small for the forbidden transitions between the low-lying levels, and that the resonances and the coupling effects arising from a large coupled-channel wave function expansion dominate the collision strengths. However, as the ion charge increases the relativistic effects become more significant. It is therefore necessary to carry out detailed calculations to determine precisely the extent of these effects in conjunction with the already complex electron correlation effects, as manifested in particular in autoionising resonances. Similar to the calculations described by Zhang (1996, IP Paper XVIII), we have carried out several sets of NR and BPRM calculations, including a 19-level BPRM calculation (or 19BP for brevity), a 8-term NR calculation (8CC for brevity), and a large 34-term (80 fine structure levels) NR CC calculation (hereafter 34CC) for Fe VI neglecting the relativistic intermediate coupling effects. In addition, we also investigate the effect on low-lying transitions by using the relativistic term coupling approximation (Eissner et al. 1974) that is often employed in close coupling and distorted wave calculations to deal with complicated ions where a full BP calculation may be difficult.

The Maxwellian-averaged rate coefficients or effective collision strengths are calculated and tabulated over a temperature range in which Fe VI is most abundant in astrophysical sources. A brief description of the computations and the results are given in the following section.

The present work is part of an international collaboration referred to as the IRON Project (Hummer et al. 1993, Paper I) to obtain accurate electron-impact excitation rates for fine-structure transitions in atomic ions. A full list of the papers in this Atomic Data from the IRON Project series published to-date is given in the references. A complete list of papers including those in press can be found at http://www.am.qub.uk/projects/iron/papers/, where abstracts are also given for each paper. Information on other works by the authors and collaborators, including photoionization and recombination of ions of iron and other elements, can be found at http://www-astronomy.mps.ohio-state.edu/∼pradhan/.

2. Atomic calculations

The target expansions in the present work are based on the 34-term wave function expansion for Fe VI developed by Bautista (1996) using the SUPERSTRUCTURE program in his non-relativistic calculations for photoionization cross sections of Fe V. The SUPERSTRUCTURE calculations for Fe VI were extended to include relativistic fine structure using the Breit-Pauli Hamiltonian (Eissner et al. 1974; Eissner 1998). The designations for the 80 levels (34 LS terms) dominated by the configurations $3d^3$, $3d^24s$ and $3d^24p$ and their observed energies

(Sugar & Corliss 1985), are shown in Table 1. These observed energies were used in the scattering Hamiltonian diagonalization to obtain the surface amplitudes at stage STGH (Berrington et al. 1995). This table also provides the key to the level indices for transitions in tabulating the Maxwellian-averaged collision strengths. The subset of 19-levels, the first 8 LS terms dominated by $3d^3$, are used in both the intermediate coupling BP and the nonrelativistic recoupling calculations, with and without the term coupling coefficients (TCC's) for the purpose of comparisons (Chen & Pradhan 1998, CP). An indication of the accuracy of the target eigenfunctions may be obtained from the calculated energy levels in Table 1 of CP and from the computed length and velocity oscillator strengths for some of the dipole fine structure transitions given in Table 2 of CP. The agreement between the length and velocity oscillator strengths is generally about 10%, an acceptable level of accuracy for a complex iron ion.

The collision calculations in the present work, as in the earlier works in Papers III, VI, XVIII and XXVII of the IP, entail the calculation of the reactance matrix (the K-matrix) which yields the collision strengths. In the NR algebraic recoupling approach, the K-matrices are obtained as usual by the different stages of the R-matrix package (Berrington et al. 1995) in LS coupling. The K-matrices are subsequently transformed from LS coupling to pair coupling (Saraph 1972, 1978), using the STGFJ code (Luo & Pradhan 1990; Zhang & Pradhan 1995a) which is an extension of the NR LS coupling asymptotic region code, STGF (Hummer et al. 1993). The collision strengths were calculated for a large number of electron energies ranging from 0 to 10 Rydbergs by 34CC. This energy range was carefully chosen in order to obtain detailed structures of collision strengths in the region where they are dominated by resonances, as well as in an extended region where resonances are not important or have not been included but which are necessary to obtain accurate Maxwellian-averaged rate coefficients for the electron temperature range of interest. As the electron Maxwellian at a given temperature is weighted towards lower energies, it is desirable and usually necessary to use a fine mesh of energies in the near-threshold region. The mesh is coarser at higher energies not only because it is weighted less in rate coefficients, but also because the calculations are more CPU time consuming as more target thresholds are accessible resulting in a higher number of open channels than at low energies.

In order to delineate the extensive near-threshold resonance structures, an effective quantum number ν-mesh was used to obtain the collision strengths at 8913 energy points in the range $E = 0 - 0.25$ Rydbergs. On this so called "quantum defect" mesh, 100 points ($\Delta\nu = 0.01$) are obtained in each interval $(\nu, \nu + 1)$. The ν-mesh ensures equal sampling of resonances in each successive interval, $(\nu, \nu + 1)$ where $\nu(E) = z/\sqrt{E_t - E}$; E_t is the energy of the particular target threshold to which the

Table 1. The 80 fine structure levels corresponding to the 34 LS terms included in the calculations and their observed energies (Ry) in Fe VI (Sugar & Corliss 1985)

i	Term		2J	Energy	i	Term		2J	Energy
1	$3d^3$	^{4}F	3	0.0	41	$3d^2(^3$F$)4p$	^{4}F$^\circ$	5	3.101443
2			5	0.004659	42			7	3.110750
3			7	0.010829	43			9	3.120492
4			9	0.018231	44	$3d^2(^3$F$)4p$	^{2}F$^\circ$	5	3.121742
5	$3d^3$	^{4}P	1	0.170756	45			7	3.131189
6			3	0.172612	46	$3d^2(^3$F$)4p$	^{4}D$^\circ$	1	3.131290
7			5	0.178707	47			3	3.127568
8	$3d^3$	^{2}G	7	0.187870	48			5	3.137250
9			9	0.194237	49			7	3.147723
10	$3d^3$	^{2}P	1	0.241445	50	$3d^2(^3$F$)4p$	^{2}D$^\circ$	3	3.140706
11			3	0.238888	51			5	3.152138
12	$3d^3$	^{2}D2	3	0.260877	52	$3d^2(^3$F$)4p$	^{2}G$^\circ$	7	3.179977
13			5	0.259568	53			9	3.189597
14	$3d^3$	^{2}H	9	0.261755	54	$3d^2(^3$P$)4p$	^{2}S$^\circ$	1	3.205891
15			11	0.266116	55	$3d^2(^3$P$)4p$	^{4}S$^\circ$	3	3.240986
16	$3d^3$	^{2}F	5	0.424684	56	$3d^2(^1$D$)4p$	^{2}P$^\circ$	1	3.272354
17			7	0.421163	57			3	3.260106
18	$3d^3$	^{2}D1	3	0.656558	58	$3d^2(^1$D$)4p$	^{2}F$^\circ$	5	3.265386
19			5	0.653448	59			7	3.279505
20	$3d^2(^3$F$)4s$	^{4}F	3	2.386075	60	$3d^2(^3$P$)4p$	^{4}D$^\circ$	1	3.275057
21			5	2.390877	61			3	3.278569
22			7	2.397871	62			5	3.287005
23			9	2.406823	63			7	3.301248
24	$3d^2(^3$F$)4s$	^{2}F	5	2.452586	64	$3d^2(^1$D$)4p$	^{2}D$^\circ$	3	3.297495
25			7	2.466551	65			5	3.304281
26	$3d^2(^1$D$)4s$	^{2}D	3	2.562646	66	$3d^2(^3$P$)4p$	^{4}P$^\circ$	1	3.316518
27			5	2.559763	67			3	3.320593
28	$3d^2(^3$P$)4s$	^{4}P	1	2.565008	68			5	3.330627
29			3	2.570092	69	$3d^2(^1$G$)4p$	^{2}G$^\circ$	7	3.326827
30			5	2.578448	70			9	3.328555
31	$3d^2(^3$P$)4s$	^{2}P	1	2.623713	71	$3d^2(^3$P$)4p$	^{2}D$^\circ$	3	3.376592
32			3	2.630266	72			5	3.376970
33	$3d^2(^1$G$)4s$	^{2}G	7	2.663908	73	$3d^2(^1$G$)4p$	^{2}H$^\circ$	9	3.390785
34			9	2.663752	74			11	3.405461
35	$3d^2(^1$S$)4s$	^{2}S	1	3.065870	75	$3d^2(^3$P$)4p$	^{2}P$^\circ$	1	3.408944
36	$3d^2(^3$F$)4p$	^{4}G$^\circ$	5	3.082420	76			3	3.412018
37			7	3.093542	77	$3d^2(^1$G$)4p$	^{2}F$^\circ$	5	3.454410
38			9	3.106829	78			7	3.444151
39			11	3.123191	79	$3d^2(^1$S$)4p$	^{2}P$^\circ$	1	3.719860
40	$3d^2(^3$F$)4p$	^{4}F$^\circ$	3	3.094115	80			3	3.739745

resonance series converges. In the energy region $E = 0.25 - 10$ Rydbergs, a constant energy mesh was used. A practical reason for terminating the ν-mesh at 0.25 Rydberg is that it would take considerably more computing time and memory resources, owing to a large number of additional open channels at higher energies. The calculations are therefore optimised so as to obtain extensive delineation of resonances for the collision strengths for forbidden transitions in the low energy region that contributes predominantly to the Maxwellian rate coefficient. For the optically allowed transitions, the dominant contribution may arise from higher partial waves and higher energy regions since $\Omega \sim \ln(\epsilon)$ where resonances are relatively less important.

It is convenient to divide the overall calculation into groups of total (e + ion) symmetries $SL\pi$ according to their multiplicity, i.e. $(2S + 1) = 1, 3$, and 5 (L and S are the corresponding total orbital and spin angular momenta). Following algebraic calculations at the R-matrix STG2 stage in LS coupling, the $SL\pi$ symmetries are then recoupled in the program RECUPD to obtain total $J\pi$ (where $J = L + S$). At low impact electron energies, especially for forbidden transitions between the low-lying

levels in Fe VI, contributions to the collision strengths from total symmetries $J\pi$ with small J are dominant and those from large J are negligible. We calculated partial wave contributions from total angular momenta of the (e + ion) system with $J = 0 - 15$. The corresponding SL's (for both even and odd parities) included are

$0 \leq L \leq 15, (2S+1) = 1$
$0 \leq L \leq 16, (2S+1) = 3$
$0 \leq L \leq 17, (2S+1) = 5.$

The sum over the symmetries included should be sufficient to ensure convergence of the total collision strengths for most of the non-dipole transitions. As in several earlier calculations (e.g. for Fe IV, Zhang & Pradhan 1995a), Coulomb-Bethe (CBe) approximation was employed to account for the large ℓ contributions to supplement the collision strengths for optically allowed transitions in the energy range $0 - 10$ Rydbergs. As the ion abundance peak of Fe VI in stellar sources is at the temperature 200 000 K (Arnaud & Rothenflug 1985), the collision strengths were calculated for energy range $10 - 100$ Rydbergs or so for optically allowed transitions by CBe approach and for forbidden transitions by linking a tail with $1/\epsilon$ decrease in collision strengths. The electric dipole fine structure oscillator strengths required for CBe top-up were obtained from the BP SUPERSTRUCTURE calculations (as given in Table 2 of CP for selected transitions).

At the STG2 stage of the R-matrix calculations, it is required to specify the $(N+1)$-electron configurations that constitute the bound channel terms Φ_j's in the wave function expansion. However, the computer time and memory of the calculation are dependent on the number of such configurations included. A judicious choice needs to be made depending on whether any given particular configuration is important in the calculations or not. Therefore, in addition to those configurations required by the orthogonality condition between the continuum orbitals and the bound target orbitals, a number of complete trial calculations were carried out to select the full set of bound channel configurations employed in the present calculations. Especially, those configurations with open 3p subshell ($3p^4$ or $3p^5$) have noticeably influence on the results (the very broad near-threshold resonance features). Table 3 of CP lists these configurations according to even and odd parity. The earlier CP paper also gives a discussion of the bound channel configurations and associated resonance structures.

3. Results

In this section we present a small sample of the fine structure collision strengths in three different approximations: (a) 19BP, (b) 8CC, and (c) 34CC, and compare their Maxwellian-averaged collision strengths (the term coupling results, 8CC+TCC, are not considered as they are found to be nearly identical with the NR 8CC results).

The extensive resonance structures are displayed in Figs. 1 for the collision strengths for the first transition $\Omega(^4F_{3/2} - {}^4F_{5/2})$. As mentioned in the previous section, the mesh is considerably more refined in the low energy region $E < 0.25$ Rydberg, than at higher energies, so as to resolve accurately the near threshold resonances. The 8CC and the 34CC calculations assume degenerate fine structure level energies belonging to a given LS term, whereas the 19BP calculation employs observed energies. The 19BP results in Fig. 1a differ in detail from the 8CC and the 34CC results (Figs. 1b,c), both of which are very nearly the same, as expected for low-lying transitions; the differences are only expected to manifest themselves at higher energies owing to additional target states in the larger 34CC calculation. Figures 1b and 1c are nearly identical up to about 0.4 Rydberg. The 19BP calculations show significantly different positions and shapes for the individual features. The dense resonance structures and the background collision strengths appear consistent, so except at the low temperatures where there is no abundance of Fe VI in astronomical objects and transitions between very high-lying levels the averaged collision strengths are almost not influenced by relativistic effects, as seen from the comparisons in Tables 2 and 3 (described below).

Figures 2 present further examples of resonances in other transition $^4F_{3/2} - {}^4F_{7/2}$ within the ground term. One main feature is highlighted. In Figs. 2a–c the near-threshold region is full of dense resonances as in Figures 1, but the elevated background at low energies $E < 0.25$ Rydbergs is more pronounced relative to higher energies. The reason for the high density of resonances in this low energy range is the presence of a number of closely spaced thresholds (Table 1) that give rise to several overlapping Rydberg series of resonances.

The dominant role of resonances is clear, particularly compared to the two earlier calculations by Nussbaumer & Storey (1978) and Garstang et al. (1978), which correspond only to the non-resonant background. The Nussbaumer and Story calculations were in DW approximation that does not enable a treatment of resonances. However, the Garstang et al. calculations were in the close coupling approximation using a small basis set (Garstang et al. 1978), but they did not obtain the resonance structures and presented only averaged values (these are denoted as asterisks near the threshold energy). The computed rate coefficients are higher by several factors in comparision with the earlier collision strengths. For example, the rate coeffcient for the transition $^4F_{3/2} - {}^4F_{5/2}$ (Table 1, first transition) is approximately a factor of 5 higher (at 20 000 K) than the previous collision strengths shown in Fig. 1c. For the $^4F_{3/2} - {}^4F_{7/2}$ transition the differences with previous data are about a factor of 7.

Because of the larger target expansion in the 34CC case (as shown in Fig. 7 of CP), there are more extensive resonance structures in the 34CC case compared to the 19BP or the 8CC case at high impact energies.

Table 2. Comparison of the effective collision strengths $\Upsilon_{ij}(T)$ at 3 temperatures which cover the abundance of Fe VI in *photoionized* H II regions, from the 8CC calculation, the 19BP calculation and the 34CC calculation. i and j, referred to Table 1, are the initial and final levels

Transition		$T = 20\,000$ K			$T = 30\,000$ K			$T = 60\,000$ K		
i	j	8CC	19BP	34CC	8CC	19BP	34CC	8CC	19BP	34CC
1	2	2.54e+0	2.50e+0	2.53e+0	2.29e+0	2.23e+0	2.31e+0	1.83e+0	1.76e+0	1.91e+0
1	3	1.54e+0	1.60e+0	1.54e+0	1.35e+0	1.37e+0	1.36e+0	9.91e−01	9.73e−01	1.03e+0
1	4	1.39e+0	1.63e+0	1.38e+0	1.26e+0	1.39e+0	1.25e+0	9.42e−01	9.83e−01	9.50e−01
1	5	2.27e−01	2.25e−01	2.17e−01	2.21e−01	2.27e−01	2.16e−01	2.07e−01	2.20e−01	2.12e−01
1	6	3.25e−01	3.35e−01	3.18e−01	3.13e−01	3.32e−01	3.11e−01	2.84e−01	3.08e−01	2.92e−01
1	7	2.66e−01	2.60e−01	2.72e−01	2.53e−01	2.53e−01	2.63e−01	2.26e−01	2.27e−01	2.45e−01
1	8	7.29e−01	7.81e−01	7.03e−01	7.04e−01	7.47e−01	6.89e−01	6.50e−01	6.81e−01	6.50e−01
1	9	2.56e−01	4.17e−01	2.58e−01	2.44e−01	3.81e−01	2.50e−01	2.10e−01	3.11e−01	2.23e−01
1	10	1.33e−01	3.19e−01	1.32e−01	1.31e−01	3.00e−01	1.31e−01	1.19e−01	2.59e−01	1.20e−01
1	11	1.05e−01	1.49e−01	1.06e−01	1.04e−01	1.40e−01	1.06e−01	9.58e−02	1.18e−01	1.00e−01
2	3	3.82e+0	4.23e+0	3.82e+0	3.47e+0	3.69e+0	3.50e+0	2.75e+0	2.81e+0	2.86e+0
2	4	2.42e+0	2.78e+0	2.42e+0	2.16e+0	2.36e+0	2.17e+0	1.60e+0	1.66e+0	1.64e+0
2	5	2.73e−01	2.60e−01	2.65e−01	2.65e−01	2.58e−01	2.61e−01	2.46e−01	2.42e−01	2.49e−01
2	6	4.71e−01	4.75e−01	4.61e−01	4.56e−01	4.70e−01	4.53e−01	4.19e−01	4.40e−01	4.35e−01
2	7	4.82e−01	4.78e−01	4.85e−01	4.61e−01	4.64e−01	4.71e−01	4.14e−01	4.18e−01	4.40e−01
2	8	9.12e−01	1.03e+0	8.82e−01	8.81e−01	9.78e−01	8.63e−01	8.10e−01	8.79e−01	8.11e−01
2	9	5.68e−01	7.61e−01	5.60e−01	5.47e−01	7.09e−01	5.45e−01	4.91e−01	6.02e−01	4.98e−01
2	10	1.66e−01	4.37e−01	1.65e−01	1.64e−01	4.11e−01	1.64e−01	1.50e−01	3.58e−01	1.51e−01
2	11	1.91e−01	1.99e−01	1.92e−01	1.89e−01	1.86e−01	1.91e−01	1.75e−01	1.59e−01	1.80e−01
3	4	5.03e+0	5.62e+0	5.03e+0	4.50e+0	4.80e+0	4.55e+0	3.46e+0	3.54e+0	3.60e+0
3	5	2.59e−01	2.33e−01	2.57e−01	2.48e−01	2.30e−01	2.49e−01	2.21e−01	2.11e−01	2.31e−01
3	6	5.67e−01	5.48e−01	5.58e−01	5.51e−01	5.38e−01	5.49e−01	5.09e−01	5.02e−01	5.30e−01
3	7	8.08e−01	8.13e−01	8.01e−01	7.78e−01	7.90e−01	7.81e−01	7.07e−01	7.18e−01	7.38e−01
3	8	8.77e−01	1.06e+0	8.55e−01	8.46e−01	9.93e−01	8.34e−01	7.70e−01	8.66e−01	7.76e−01
3	9	1.09e+0	1.27e+0	1.07e+0	1.05e+0	1.20e+0	1.04e+0	9.51e−01	1.06e+0	9.70e−01
3	10	1.59e−01	4.64e−01	1.59e−01	1.58e−01	4.36e−01	1.58e−01	1.45e−01	3.77e−01	1.47e−01
3	11	3.17e−01	2.04e−01	3.18e−01	3.13e−01	1.93e−01	3.16e−01	2.87e−01	1.68e−01	2.94e−01
4	5	1.95e−01	1.68e−01	2.03e−01	1.85e−01	1.65e−01	1.95e−01	1.63e−01	1.52e−01	1.82e−01
4	6	5.45e−01	5.09e−01	5.48e−01	5.20e−01	4.85e−01	5.30e−01	4.65e−01	4.30e−01	4.92e−01
4	7	1.30e+0	1.28e+0	1.27e+0	1.26e+0	1.24e+0	1.25e+0	1.16e+0	1.14e+0	1.20e+0
4	8	5.49e−01	8.06e−01	5.51e−01	5.24e−01	7.25e−01	5.34e−01	4.53e−01	5.83e−01	4.78e−01
4	9	1.92e+0	2.01e+0	1.86e+0	1.86e+0	1.92e+0	1.81e+0	1.72e+0	1.71e+0	1.70e+0
4	10	9.73e−02	3.18e−01	1.00e−01	9.63e−02	3.03e−01	1.00e−01	8.97e−02	2.62e−01	9.63e−02
4	11	4.97e−01	1.40e−01	4.95e−01	4.92e−01	1.33e−01	4.92e−01	4.51e−01	1.17e−01	4.56e−01
5	6	3.54e−01	3.03e−01	5.06e−01	3.51e−01	3.08e−01	4.59e−01	3.37e−01	3.04e−01	4.12e−01
5	7	3.41e−01	3.19e−01	3.81e−01	3.39e−01	3.22e−01	3.69e−01	3.13e−01	3.02e−01	3.44e−01
5	8	2.84e−01	2.97e−01	2.93e−01	2.61e−01	2.73e−01	2.73e−01	2.13e−01	2.25e−01	2.29e−01
5	9	1.52e−01	1.93e−01	1.61e−01	1.40e−01	1.75e−01	1.51e−01	1.12e−01	1.36e−01	1.23e−01
5	10	6.05e−02	1.13e−01	6.28e−02	6.12e−02	1.13e−01	6.42e−02	6.05e−02	1.07e−01	6.54e−02
5	11	5.80e−02	7.77e−02	5.96e−02	5.96e−02	7.52e−02	6.14e−02	5.90e−02	7.10e−02	6.20e−02
6	7	8.19e−01	7.39e−01	1.03e+0	8.13e−01	7.43e−01	9.69e−01	7.67e−01	7.17e−01	8.86e−01
6	8	4.59e−01	5.16e−01	4.76e−01	4.23e−01	4.77e−01	4.44e−01	3.44e−01	3.89e−01	3.71e−01
6	9	4.12e−01	4.94e−01	4.31e−01	3.80e−01	4.52e−01	4.03e−01	3.06e−01	3.61e−01	3.33e−01
6	10	9.56e−02	2.37e−01	9.92e−02	9.68e−02	2.35e−01	1.02e−01	9.51e−02	2.23e−01	1.03e−01
6	11	1.41e−01	1.49e−01	1.46e−01	1.44e−01	1.41e−01	1.50e−01	1.43e−01	1.28e−01	1.51e−01
7	8	4.18e−01	4.89e−01	4.40e−01	3.87e−01	4.45e−01	4.12e−01	3.12e−01	3.47e−01	3.39e−01
7	9	8.89e−01	9.93e−01	9.21e−01	8.17e−01	9.05e−01	8.59e−01	6.65e−01	7.22e−01	7.18e−01
7	10	8.00e−02	3.14e−01	8.29e−02	8.13e−02	3.04e−01	8.54e−02	7.84e−02	2.82e−01	8.62e−02
7	11	2.75e−01	1.25e−01	2.84e−01	2.82e−01	1.20e−01	2.91e−01	2.82e−01	1.10e−01	2.96e−01
8	9	3.00e+0	2.72e+0	4.83e+0	2.76e+0	2.52e+0	4.00e+0	2.28e+0	2.11e+0	2.97e+0
8	10	3.44e−01	8.51e−01	3.43e−01	3.48e−01	7.99e−01	3.46e−01	3.18e−01	6.48e−01	3.22e−01
8	11	4.81e−01	5.58e−01	4.82e−01	4.86e−01	5.26e−01	4.84e−01	4.41e−01	4.30e−01	4.48e−01
9	10	2.74e−01	8.63e−01	2.76e−01	2.77e−01	8.25e−01	2.77e−01	2.50e−01	7.13e−01	2.56e−01
9	11	7.54e−01	3.03e−01	7.55e−01	7.62e−01	2.91e−01	7.61e−01	6.95e−01	2.52e−01	7.07e−01
10	11	3.29e−01	3.14e−01	3.23e−01	3.22e−01	2.90e−01	3.19e−01	2.93e−01	2.44e−01	3.08e−01

Consequently, as seen below, the 34CC rate coefficients should show a larger resonance enhancement especially at high electron temperatures.

The procedure for obtaining the Maxwellian-averaged collision strength, or the effective collision strength, can be found in earlier publications in this series (e.g. see Papers I, VI or XVIII). This quantity is defined as

$$\Upsilon_{ij} = \int_0^\infty \Omega_{ij} e^{-\epsilon_j/kT} d(\epsilon_j/kT). \tag{1}$$

Fe VI is abundant in H II regions at around 20 000 K (Hyung & Aller 1997), and in collisionally ionized coronal type sources at around 200 000 K (Arnaud & Rothenflug

Table 3. Comparison of the effective collision strengths $\Upsilon_{ij}(T)$ at 3 temperatures which cover the peak abundance of Fe VI in *coronal* plasmas sources, from the 8CC calculation, the 19BP calculation and the 34CC calculation. i and j, referred to Table 1, are the initial and final levels

Transition		T = 100 000 K			T = 200 000 K			T = 300 000 K		
i	j	8CC	19BP	34CC	8CC	19BP	34CC	8CC	19BP	34CC
1	2	1.53e+0	1.47e+0	1.66e+0	1.22e+0	1.18e+0	1.43e+0	1.08e+0	1.07e+0	1.31e+0
1	3	7.51e−01	7.33e−01	8.20e−01	5.09e−01	5.04e−01	6.25e−01	4.13e−01	4.15e−01	5.34e−01
1	4	7.00e−01	7.15e−01	7.30e−01	4.43e−01	4.44e−01	5.05e−01	3.37e−01	3.35e−01	4.05e−01
1	5	1.96e−01	2.12e−01	2.14e−01	1.84e−01	2.02e−01	2.17e−01	1.79e−01	1.92e−01	2.13e−01
1	6	2.59e−01	2.81e−01	2.81e−01	2.36e−01	2.44e−01	2.70e−01	2.31e−01	2.25e−01	2.59e−01
1	7	2.00e−01	2.00e−01	2.31e−01	1.71e−01	1.65e−01	2.10e−01	1.62e−01	1.47e−01	1.92e−01
1	8	5.93e−01	6.18e−01	6.08e−01	5.16e−01	5.41e−01	5.42e−01	4.79e−01	5.08e−01	4.98e−01
1	9	1.78e−01	2.57e−01	1.96e−01	1.38e−01	1.98e−01	1.59e−01	1.20e−01	1.74e−01	1.39e−01
1	10	1.05e−01	2.28e−01	1.10e−01	8.77e−02	1.97e−01	9.53e−02	7.91e−02	1.87e−01	8.65e−02
1	11	8.71e−02	9.99e−02	9.47e−02	7.74e−02	8.07e−02	8.65e−02	7.45e−02	7.39e−02	8.02e−02
2	3	2.25e+0	2.28e+0	2.46e+0	1.74e+0	1.77e+0	2.06e+0	1.52e+0	1.56e+0	1.85e+0
2	4	1.20e+0	1.23e+0	1.28e+0	7.95e−01	7.96e−01	9.39e−01	6.28e−01	6.24e−01	7.85e−01
2	5	2.30e−01	2.25e−01	2.45e−01	2.15e−01	2.04e−01	2.40e−01	2.09e−01	1.91e−01	2.32e−01
2	6	3.89e−01	4.08e−01	4.27e−01	3.61e−01	3.66e−01	4.20e−01	3.51e−01	3.41e−01	4.06e−01
2	7	3.72e−01	3.73e−01	4.19e−01	3.26e−01	3.15e−01	3.90e−01	3.12e−01	2.85e−01	3.64e−01
2	8	7.34e−01	7.87e−01	7.55e−01	6.31e−01	6.73e−01	6.70e−01	5.82e−01	6.25e−01	6.14e−01
2	9	4.33e−01	5.14e−01	4.51e−01	3.57e−01	4.14e−01	3.85e−01	3.21e−01	3.73e−01	3.45e−01
2	10	1.34e−01	3.17e−01	1.39e−01	1.13e−01	2.75e−01	1.21e−01	1.04e−01	2.61e−01	1.10e−01
2	11	1.58e−01	1.37e−01	1.68e−01	1.39e−01	1.14e−01	1.52e−01	1.32e−01	1.06e−01	1.40e−01
3	4	2.76e+0	2.78e+0	3.01e+0	2.05e+0	2.05e+0	2.45e+0	1.76e+0	1.76e+0	2.18e+0
3	5	1.97e−01	1.91e−01	2.18e−01	1.74e−01	1.64e−01	2.02e−01	1.70e−01	1.50e−01	1.88e−01
3	6	4.71e−01	4.67e−01	5.24e−01	4.26e−01	4.20e−01	5.17e−01	4.07e−01	3.93e−01	5.01e−01
3	7	6.45e−01	6.53e−01	7.12e−01	5.84e−01	5.71e−01	6.83e−01	5.66e−01	5.27e−01	6.51e−01
3	8	6.91e−01	7.60e−01	7.14e−01	5.85e−01	6.35e−01	6.25e−01	5.36e−01	5.82e−01	5.69e−01
3	9	8.51e−01	9.30e−01	8.93e−01	7.21e−01	7.79e−01	7.84e−01	6.62e−01	7.18e−01	7.17e−01
3	10	1.30e−01	3.31e−01	1.36e−01	1.13e−01	2.84e−01	1.20e−01	1.05e−01	2.67e−01	1.10e−01
3	11	2.57e−01	1.48e−01	2.73e−01	2.22e−01	1.28e−01	2.43e−01	2.07e−01	1.21e−01	2.24e−01
4	5	1.43e−01	1.35e−01	1.71e−01	1.19e−01	1.09e−01	1.55e−01	1.11e−01	9.57e−02	1.41e−01
4	6	4.16e−01	3.81e−01	4.64e−01	3.66e−01	3.19e−01	4.30e−01	3.53e−01	2.88e−01	4.01e−01
4	7	1.09e+0	1.06e+0	1.18e+0	1.02e+0	9.67e−01	1.17e+0	9.95e−01	9.08e−01	1.14e+0
4	8	3.86e−01	4.78e−01	4.23e−01	3.03e−01	3.62e−01	3.49e−01	2.65e−01	3.14e−01	3.07e−01
4	9	1.56e+0	1.53e+0	1.59e+0	1.35e+0	1.33e+0	1.42e+0	1.25e+0	1.24e+0	1.31e+0
4	10	8.26e−02	2.25e−01	9.20e−02	7.57e−02	1.83e−01	8.31e−02	7.51e−02	1.64e−01	7.47e−02
4	11	4.05e−01	1.05e−01	4.19e−01	3.46e−01	9.32e−02	3.69e−01	3.18e−01	9.04e−02	3.37e−01
5	6	3.20e−01	2.92e−01	3.96e−01	3.25e−01	2.73e−01	3.79e−01	3.60e−01	2.61e−01	3.58e−01
5	7	2.88e−01	2.81e−01	3.37e−01	2.84e−01	2.60e−01	3.36e−01	3.11e−01	2.52e−01	3.28e−01
5	8	1.75e−01	1.85e−01	1.92e−01	1.33e−01	1.40e−01	1.47e−01	1.19e−01	1.20e−01	1.23e−01
5	9	8.82e−02	1.07e−01	1.00e−01	6.40e−02	7.58e−02	7.24e−02	5.66e−02	6.25e−02	5.86e−02
5	10	5.89e−02	1.00e−01	6.54e−02	5.78e−02	9.00e−02	6.27e−02	5.89e−02	8.54e−02	5.90e−02
5	11	5.65e−02	6.79e−02	6.12e−02	5.68e−02	6.56e−02	5.82e−02	6.16e−02	6.61e−02	5.48e−02
6	7	7.25e−01	6.83e−01	8.61e−01	7.37e−01	6.38e−01	8.48e−01	8.13e−01	6.13e−01	8.20e−01
6	8	2.80e−01	3.17e−01	3.10e−01	2.14e−01	2.34e−01	2.37e−01	1.91e−01	1.97e−01	2.00e−01
6	9	2.47e−01	2.90e−01	2.76e−01	1.85e−01	2.08e−01	2.06e−01	1.65e−01	1.73e−01	1.72e−01
6	10	9.19e−02	2.08e−01	1.03e−01	9.05e−02	1.88e−01	9.91e−02	9.38e−02	1.82e−01	9.39e−02
6	11	1.37e−01	1.20e−01	1.50e−01	1.37e−01	1.16e−01	1.45e−01	1.46e−01	1.20e−01	1.38e−01
7	8	2.49e−01	2.72e−01	2.78e−01	1.84e−01	1.91e−01	2.04e−01	1.63e−01	1.57e−01	1.67e−01
7	9	5.43e−01	5.81e−01	6.01e−01	4.14e−01	4.24e−01	4.60e−01	3.71e−01	3.59e−01	3.91e−01
7	10	7.40e−02	2.61e−01	8.49e−02	7.49e−02	2.39e−01	8.11e−02	8.29e−02	2.29e−01	7.67e−02
7	11	2.75e−01	1.00e−01	2.95e−01	2.71e−01	9.16e−02	2.86e−01	2.80e−01	9.05e−02	2.73e−01
8	9	1.89e+0	1.76e+0	2.41e+0	1.44e+0	1.36e+0	1.88e+0	1.25e+0	1.18e+0	1.63e+0
8	10	2.80e−01	5.31e−01	2.94e−01	2.38e−01	4.04e−01	2.50e−01	2.26e−01	3.48e−01	2.21e−01
8	11	3.88e−01	3.53e−01	4.09e−01	3.33e−01	2.68e−01	3.52e−01	3.20e−01	2.32e−01	3.13e−01
9	10	2.20e−01	6.13e−01	2.33e−01	1.88e−01	4.99e−01	2.01e−01	1.82e−01	4.51e−01	1.79e−01
9	11	6.11e−01	2.16e−01	6.46e−01	5.19e−01	1.72e−01	5.60e−01	4.95e−01	1.49e−01	5.03e−01
10	11	2.71e−01	2.14e−01	3.10e−01	2.72e−01	1.91e−01	3.15e−01	2.99e−01	1.91e−01	3.04e−01

1992). Tables 2 and 3 correspond to these rather disparate temperature ranges. We compare the Maxwellian-averaged collision strengths, in the three approximations, for a few of the low-lying transitions at three representative temperatures for Fe VI. Surprisingly, we find that the differences between the three sets of calculations is large only for transitions between very high-lying levels or

at the lowest electron temperature, 10 000 K, when the Maxwellian samples a small energy range above threshold, typically about 1 eV or 0.1 Rydberg. At higher temperatures, considered in Tables 2 and 3, the differences are small; for example at 100 000 K the differences are no more than a few percent (Table 3). It follows that the relativistic effects are not important as far as the
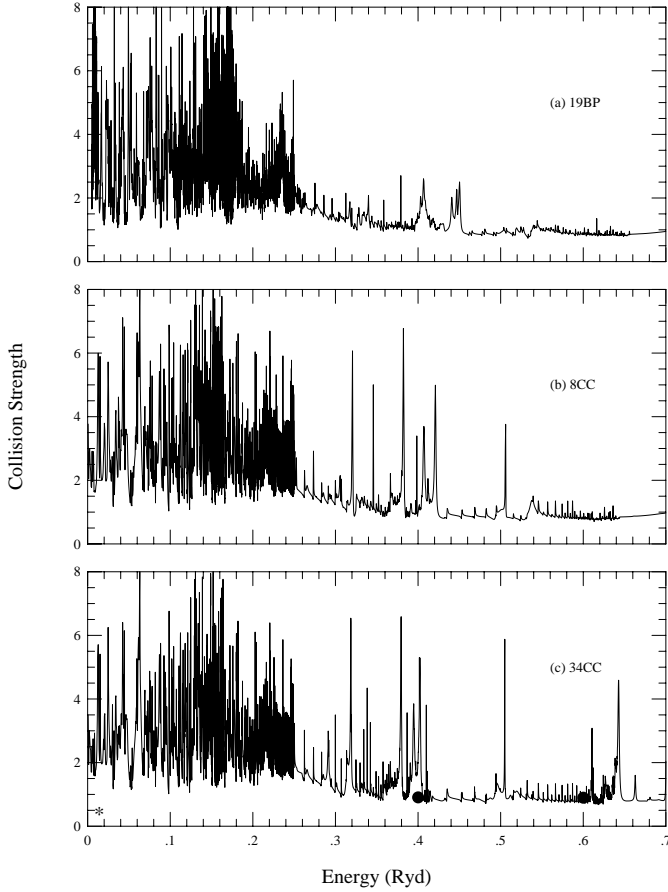
Fig. 1. Collision strengths for the first transition $\Omega(^4\mathrm{F}_{3/2} - {}^4\mathrm{F}_{5/2})$: **a)** 19BP Breit-Pauli R-matrix calculation; **b)** 8CC nonrelativistic algebraic recoupling; **c)** 34CC nonrelativistic algebraic recoupling. The "●" and the "∗" near the threshold energy were calculated by Nussbaumer & Storey (1978) and Garstang et al. (1978), respectively

Fig. 2. $\Omega(^4\mathrm{F}_{3/2} - {}^4\mathrm{F}_{7/2})$ for fine structure levels within the ground term

calculation of rate coefficient is concerned. This fact is of considerable practical significance since it implies that we can accurately compute the effective collision strengths for the low-lying transitions from among the 80 fine structure levels using the large 34CC dataset. However the fine structure effects are expected to manifest themselves more strongly for transitions among the closely spaced higher lying levels, and the uncertainties (discussed later) will be larger than for the transitions among the 19 levels explicitly studied herein. In the practical calculations of Υ_{ij} in Eq. (1), the impact energies ϵ_j go up to 100 Rydbergs instead of ∞. According to the temperatures of abundance for Fe VI in astronomical objects under coronal equilibrium, the maximum temperature is 10^6 K (Table 3). Therefore the Maxwellian factor in Eq. (1) $\mathrm{e}^{-\epsilon_j/kT} = \mathrm{e}^{-100*157885/10^6} \simeq \mathrm{e}^{-16}$, which ensures the convergence for the calculation of Eq. (1) over the full temperature range covered. However, for more highly ionized systems such as the ongoing calculation of Fe XVII, the upper bound of ϵ_j used should be at least a few hundred
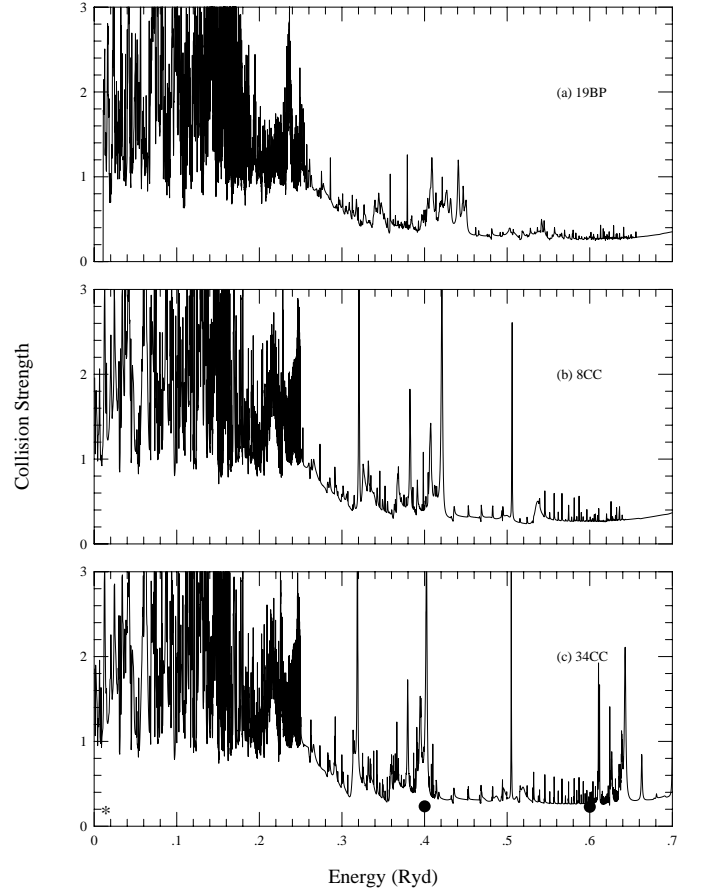
Rydbergs as the temperature of the maximum abundance of Fe XVII is 10^6 K to 10^7 K.

Figures 3 show the collision strengths for the optically allowed transitions (a) $3\mathrm{d}^3\ {}^4\mathrm{F}_{3/2} - 3\mathrm{d}^2 4\mathrm{p}\ {}^4\mathrm{G}^o_{5/2}$, (b) $3\mathrm{d}^3\ {}^4\mathrm{F}_{3/2} - 3\mathrm{d}^2 4\mathrm{p}\ {}^4\mathrm{F}^o_{3/2}$, (c) $3\mathrm{d}^3\ {}^4\mathrm{F}_{5/2} - 3\mathrm{d}^2 4\mathrm{p}\ {}^4\mathrm{G}^o_{7/2}$, and (d) $3\mathrm{d}^3\ {}^4\mathrm{F}_{7/2} - 3\mathrm{d}^2 4\mathrm{p}\ {}^4\mathrm{G}^o_{9/2}$. As mentioned earlier, the Coulomb-Bethe approximation was employed to estimate the contributions from high partial waves. It is clear from the figures that relative resonance contributions are not as strong as in the forbidden transitions and the rate coefficients are dominated by the high energy region where the collision strength has the Bethe asymptotic behavior, $\Omega \sim \ln(\epsilon)$.

As discussed in detail in the earlier work by CP on the bound channel expansion in the close coupling calculations for Fe VI, these $(N + 1)$-electron functions are found to appear as resonances in the collision strengths. Often in close coupling calculations the bound channel configurations are not well represented from the point of view of a reasonably complete configuration-interaction expansion. This is particularly the case when the continuum channel expansion over the target states does not include the same configurations as the bound channels, which can then lead to large pseudoresonances in the cross sections. However,
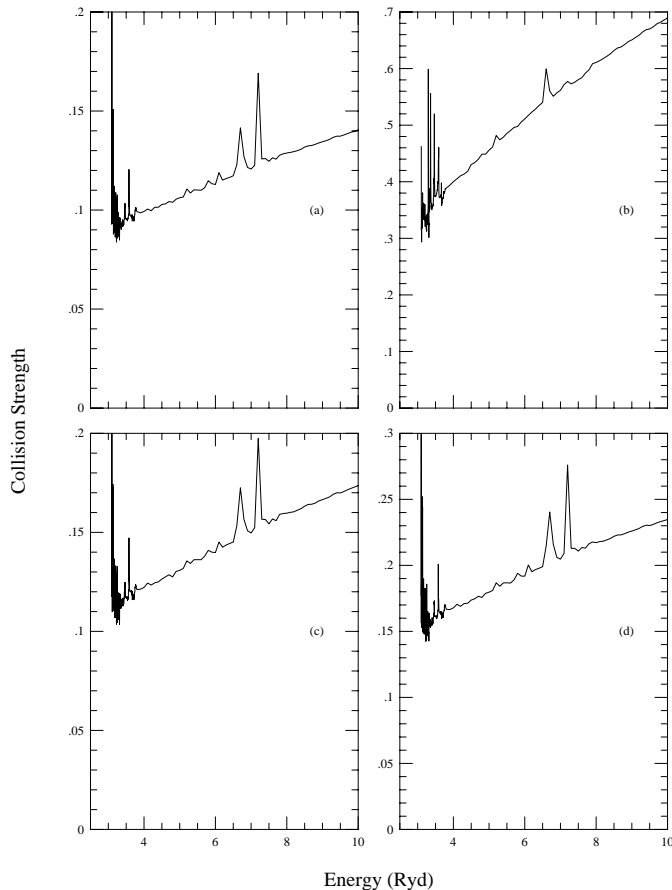
Fig. 3. The collision strengths enhanced by CBe top-up for the optically allowed transitions **a)** $3d^3 \ ^4F_{3/2} - 3d^2 4p \ ^4G^o_{5/2}$, **b)** $3d^3 \ ^4F_{3/2} - 3d^2 4p \ ^4F^o_{3/2}$, **c)** $3d^3 \ ^4F_{5/2} - 3d^2 4p \ ^4G^o_{7/2}$, and **d)** $3d^3 \ ^4F_{7/2} - 3d^2 4p \ ^4G^o_{9/2}$, from the 34CC calculation

if care is exercised in the choice of the continuum and the bound channel expansions, the latter set corresponds well to physical resonances. For example, CP find that one particular bound channel configuration $3p^5 3d^5$ leads to a considerable but diffuse rise in the near-threshold background of the collision strength $\Omega(^4F_{3/2} - {}^4F_{5/2})$ and $\Omega(^4F_{5/2} - {}^4F_{9/2})$ (Figs. 6a,b of CP are plotted with and without this configuration). We also note that such bound channel resonances were also found to have an appreciable effect in the near-threshold region in an earlier work on the photoionization of Fe IV (Bautista & Pradhan 1997).

The Maxwellian-averaged collision strengths were calculated for all 3610 non-vanishing transitions between 80 energy levels shown in Table 4 (available in electronic form) for 21 temperatures ranging from 10 000 to 100 0000 K.

4. Discussion and conclusion

Unlike the lower ionization stages of Fe, such as Fe III and Fe IV, it is found that it is necessary to explicitly consider the fine structure in the target in order to delineate precisely the positions of autoionizing resonances and detailed resonance structures. However the overall relativistic effects on the the Maxwellian-averaged collision strengths are small, and the NR and BPRM approximations yield close agreement for the forbidden transitions between the low-lying even states. Before carrying out the large-scale 34CC calculation, the test runs with the BPRM method (Berrington et al. 1995) using a 19-level target corresponding to the 8 LS terms showed that although the 19BP calculations show significant difference in the positions and shapes for the resonance features in individual transitions, the overall difference in the averaged collision strengths is small among the 19BP, 8CC and 34CC calculations. However, the smaller 8CC or the 19BP calculations entail only a small number of transitions compared to the larger 34CC calculation. Establishing that the relativistic effects are indeed not important for the calculation of the rate coefficients of Fe VI, this provided the basis for the much more extensive calculations. The algebraic recoupling method, following the NR calculations, was used to obtain results for all transitions among the 80 fine structure levels of the 34 LS terms.

Here, we give an estimate of the accuracy of the present data. An examination of Tables 2nd 3 suggests that the general level of agreement between the 3 sets of results may be used as an accuracy criterion, indicating the maximum dispersion due to numerical uncertainties associated with resolution of resonances and relativistic effects to the extent they are operative. The fine mesh was used up to $E = 0.7$ Ry and the important resonance features for transitions from the lower-lying, even-parity levels up to the $3d^3 \ ^2D1^o_J$ levels are fully resolved so rate coefficients for this type of transitions should be highly accurate, $\approx 10 - 20\%$. For optically allowed transitions from the low-lying levels to the odd parity levels with energies below 0.7 Ry, the rate coefficients should also be of the same accuracy since resonances are relatively less important and the collision strengths are large and dominated by the higher partial waves, as seen from Fig. 3. For the other forbidden (and inter-combination) transitions between these intermediate-energy levels, the accuracy of the rate coefficients is expected to be less, $\approx 30 - 50\%$. For transitions corresponding to excitation to the high-lying levels with threshold energies greater than 2.8 Ry, the uncertainty could exceed 50% since a coarse energy mesh was used and the resonances and coupling effects due to higher terms were neglected. We would also emphasize here that for all transitions the Maxwellian-averaged collision strengths for high temperatures (roughly higher than the highest threshold energy included in the target expansion, about 400 000 K in the present case) could have a larger uncertainty, since resonances due to higher target states are not included. However, data at temperatures much higher than these are of little astrophysical

interest. This general criterion should apply to all our earlier publications in this series.

The present work will hopefully provide a reasonably complete collisional dataset for extensive astrophysical diagnostics of Fe VI spectra from various sources. Further work is planned on the forbidden transition probabilities of [Fe VI], and on computation of line ratios using the collisional and radiative datasets. An electronic data table of all the non-vanishing Maxwellian-averaged collision strengths between the 80 fine structure levels constitutes Table 4 of the present work. As Table 4 is rather voluminous it is available in electronic form from the CDS or via ftp from the authors at: chen@astronomy.ohio-state.edu.

References

Arnaud M., Rothenflug R., 1985, A&AS 60, 425

Bautista M.A., 1996, A&AS 119, 105 (Paper XVI)

Bautista M.A., Pradhan A.K., 1997, A&AS 126, 365 (Paper XXVI)

Berrington K.A., Eissner W.B., Norrington P.H., 1995, Comp. Phys. Comm. 92, 290

Chen G.X., Pradhan A.K., 1998, J. Phys. B (submitted CP)

Eissner W., 1998, Comput. Phys. Commun 114, 295

Eissner W., Jones M., Nussbaumer H., 1974, Comput. Phys. Commun 8, 270

Garstang R.H., Robb W.D., Rountree S.P., 1978, ApJ 222, 384

Hummer D.G., Berrington K.A., Eissner W., et al., 1993, A&A 279, 298 (Paper I)

Hyung S., Aller L.H., 1997, MNRAS 292, 71

Jordan S., Koester D., Finley D., 1995, in Astrophysics in the Extreme Ultraviolet, Bowyer S. and Malina R.F. (eds.). Kluwer Academic Press

Koester D., 1995, in Astrophysics in the Extreme Ultraviolet, Bowyer S. and Malina R.F. (eds.). Kluwer Academic Press

Luo D., Pradhan A.K., 1990, Phys. Rev. A 41, 165

Nussbaumer H., Storey P.J., 1978, A&A 70, 37

Pradhan A.K., 1994, At. Data Nucl. Data Tab. 57, 297

Saraph H.E., 1972, Comput. Phys. Commun. 3, 256

Saraph H.E., 1978, Comput. Phys. Commun. 15, 247

Sugar J., Corliss C., 1985, J. Phys. Chem. Ref. Data 14, Suppl. 2

Zhang H.L., 1996, A&AS 119, 523 (Paper XVIII)

Zhang H.L., Graziani M., Pradhan A.K., 1994, A&A 283, 319 (Paper III)

Zhang H.L., Pradhan A.K., 1995a, J. Phys. B 28, 3403

Zhang H.L., Pradhan A.K., 1995b, A&A 293, 953 (Paper VI)

Zhang H.L., Pradhan A.K., 1997, A&AS 126, 373 (Paper XXVII)